

HEAVY-ION BEAM DYNAMICS IN THE RIA ACCELERATORS*

P.N. Ostroumov

Physics Division, Argonne National Laboratory, 9700 S. Cass Avenue, Argonne, IL, 60439

Abstract

The Rare-Isotope Accelerator (RIA) Project includes a cw 1.4 GV driver linac and a 123 MV post-accelerator both based on SC cavities operating at frequencies from 48 MHz to 805 MHz. Several new conceptual solutions in the physics design of heavy-ion SC linacs have been developed recently. Particularly, the concept of multiple charge state beam acceleration in SC linacs has been tested and will be used in the RIA driver linac to increase available accelerated beam power. A detailed design has been developed for the focusing-accelerating lattice of the RIA linacs which are configured as an array of short SC cavities, each with independently controllable rf phase. Independent phasing allows the velocity profile to be varied so that the linac can be tuned to provide higher energies for the lighter ions. For example, the reference design linac can be tuned to provide a uranium beam at an energy of 403 MeV/u and can be re-tuned to provide a proton beam at 900 MeV.

To obtain 403 MeV/u uranium beams the driver linac uses two strippers which separate three different sections of the linac. The low- β section of the linac is that portion prior to the first stripper, the medium- β section is that between the two strippers, and the high- β section is that portion following the second stripper. The low- β section includes a high-intensity Electron Cyclotron Resonance (ECR) ion source, an achromatic 120° bend and a Low Energy Beam Transport with the possibility to accept for acceleration two-charge states simultaneously, a Radio Frequency Quadrupole, a Medium Energy Beam Transport and a SC linac up to ~9.5 MeV/u for uranium. The medium- β and high- β section are designed for acceleration of multiple charge state beams. After each stripper there is a magnetic transport system which provides six-dimensional matching of multiple charge state beams to the following accelerating structure. In order to avoid beam losses in the high-energy section of the Driver Linac the low-intensity unwanted charge states must be carefully separated and dumped. This magnetic transport system requires focusing, dipole, sextupole magnets and a rebuncher in order to provide a proper transformation of the 6-dimensional beam emittance.

Beam dynamics studies have been performed with the goal of optimization of the linac structure in order to reduce any effective emittance growth of the multi-q uranium beam. The dynamics of single- and multiple-charge state beams are detailed, including the effects of possible errors in rf field parameters and misalignments of transverse focussing elements. Several computer codes were applied for the design of the driver linac. Beam parameters of ECR ion sources were adapted from recent experimental data and with an extrapolation to higher intensities based on estimates of the VENUS Ion Source group.

Comparison of beam dynamics performance in the high-beta section of the RIA driver linac has been done for two types of accelerating structures: one using elliptical cavities as in the baseline proposal and one based on triple-spoke cavities.

* Work supported by the U. S. Department of Energy under contract W-31-109-ENG-38.

I. GENERAL LAYOUT OF THE RIA DRIVER LINAC

The principal requirements for a high-power medium energy SC accelerator are that it be capable of producing beams of any ion, including uranium, at energies of 400 MeV/nucleon and a total beam power of 400 kW. A conceptual design for such a linac has been developed for the RIA project, the major elements of which are shown in Fig. 1. Except for the injector RFQ, the entire linac is based on superconducting (SC) accelerating structures, which not only enable cost-effective cw operation, but also, as discussed below, have numerous additional advantages for this application. The baseline design of the linac contains 9 types of SRF accelerating cavities. The layout, configuration, and many details of the RIA driver linac have been discussed and presented at several conferences and workshops [1,2,3,4]. Beam dynamics studies in the baseline design of the driver linac were presented in ref. [5].

The longitudinal and transverse acceptance of the high- β section is ~ 100 times larger than the input beam emittance, which is determined by the ion source and injector RFQ. Such an immense margin for emittance growth makes possible a novel operating mode for the linac, in which the beam contains multiple charge-states [6, 7]. By simultaneously accelerating several of the charge states resulting from stripping the beam, a much higher fraction of the stripped beam can be utilized. The increase in efficiency not only provides a substantial increase in the available beam current, but also enables the use of multiple strippers, reducing the size of the linac required for 400 MeV/u beams. A third benefit of using multiple charge states is a reduction in the amount of beam dumped during charge-state selection at the stripping points: this in turn reduces shielding requirements. As discussed in ref. [5,6,7], full 3D numerical simulations show such operation to be straightforward, entailing a modest increase of longitudinal and transverse emittance, which remains well within the linac acceptance. Also, it should be noted that the feasibility of multiple charge-state (multi-q) beam acceleration has been experimentally established in a series of tests with the existing SC ion accelerator ATLAS [8]. In addition, it was shown that the Front End of the driver linac can be designed for the acceptance of two charge states of uranium beam from the ECR ion source, doubling the available uranium beam power [9].

The driver linac is a high intensity machine and relative beam losses in the high-energy section must be kept below 10^{-4} . Acceleration of multi-q uranium beam places stringent requirements on the linac design. All other lighter ion beams can be accelerated with even smaller emittances. Below we present beam dynamics studies which have been performed with the goal of optimization of the linac structure in order to reduce a possible effective emittance growth of multi-q uranium beam.

II. LINAC DESIGN CODES

Several computer codes were applied for the design of the driver linac. Beam parameters of ECR ion sources were adapted from the recent experimental data and an extrapolation to higher intensities based on estimates of VENUS Ion Source group [10]. For the design of beam transport lines the codes GIOS [11], COSY [12] and TRANSPORT [13], were used. An RFQ capable of accelerating two charge-state uranium beam was designed using the DYNAMION code [14]. Beam dynamics design and optimization along the SRF linac was performed using the TRACK code [15]. Beam transport codes which include higher order terms such as GIOS and COSY were applied for the design of multi-q beam transitions and switchyard.

The code TRACK has been written in order to integrate charged particle motion in the presence of all components of the electromagnetic field. Full 3D electromagnetic fields in all SRF cavities were obtained from the code CST Microwave Studio (MWS) [16]. The MWS code running on modern PCs can calculate all six components of an electromagnetic field distribution within the beam-cavity interaction area with a mesh size of less than 1 mm. The TRACK integrates the equation of motion by 4th order Runge-Kutta method. Static and electromagnetic fields of the accelerator elements are three-dimensional. The fringing fields are included following the codes RAYTRACE [17] and COSY [12].

Beam dynamics simulation in each of three sections of the driver linac included the following steps:

- Beam matching in transverse and longitudinal phase spaces for a trial beam with the mean value of charge-to-mass ratio. Simulation of the trial ion beam to minimize beam sizes, to obtain smooth rms envelopes in transverse planes. The rms oscillations in longitudinal phase space due to the effect of inter-cavity drift spaces and specific linac lattice were minimized by adjusting cavity synchronous phases.
- Simulation of multi-q beams. Final determination of beam energies at stripping foil and total required number of the cavities. Higher order optimization of the multi-q transitions between the accelerator sections.
- Beam dynamics simulation of the multi-q beam under the effect of random errors both in transverse and longitudinal phase space.

III. FRONT END OF THE DRIVER LINAC

The initial acceleration of heavy-ion beams in the driver linac will be provided by a room temperature RFQ operating at 57.5 MHz [18]. The primary scope of the RFQ is the acceleration of low longitudinal emittance dual charge state uranium beams. Transverse emittance should remain unchanged and a high beam capture efficiency is required. In order to simplify the front end of multi-beam driver linac and accommodate different ion species from the ECR ion source the RFQ must operate at a wide range of power levels. The basic RFQ parameters are listed in Table I. As was discussed in our previous work [9], a multi-harmonic buncher must be used upstream of the RFQ to produce the lowest possible longitudinal emittance of two charge state beams. The ion beam distribution in the longitudinal phase space at the RFQ entrance is determined by a four-harmonic buncher, and is shown in Fig. 2. The central part of the distribution contains more than 80% of the particles within a phase width equal to $\pm 25^\circ$. The main goal of the beam dynamics design is to accept the core of the initial distribution and reliably eliminate halo particles from the acceleration process. This can be done if the acceleration starts with a small separatrix whose length is kept constant along the RFQ. The condition $\frac{T \sin \varphi_s}{\beta^2} = const$ ensures that all particle trajectories in phase space are conserved in

the linear approximation. T is the RFQ accelerating efficiency, β is the particle relative velocity and φ_s is the synchronous phase. A strong coupling of the longitudinal and transverse motions in the front end of the RFQ is an inherent property of heavy-ion RFQs. The Hamiltonian for longitudinal motion in an RFQ can be expressed as [19]:

$$H(\Delta z, \Delta \beta) = \frac{c\Delta\beta^2}{2} + \frac{qeU_0T}{\pi AW_u} \left(k\Delta z \cos \varphi_s - I_0^2 \left(\frac{kR}{2} \right) \sin(k\Delta z - \varphi_s) \right), \quad (1)$$

where Δz , Δp are particle coordinates with respect to the reference particle in phase space, qe is the ion charge, $W_u = m_u c^2$, m_u is the atomic unit mass, A is the mass number, c is the speed of light, U_0 is the vane-to-vane voltage, R is the average amplitude of transverse oscillations, and I_0 is the modified Bessel function. In the front end of the RFQ the term $I_0(kR/2)$ is not small and the Hamiltonian strongly depends on amplitude of transverse oscillations. Figure 2 shows the separatrices calculated for the initial value of the synchronous particle velocity $\beta = 0.00507$ for different amplitudes of the transverse oscillations. The initial values of T and φ_s can be chosen to accept the central dense area of the initial distribution into the separatrix corresponding to $R=0$. However, there are particles with large transverse amplitudes. These particles are captured for acceleration and have large longitudinal amplitudes. Obviously, they form a halo in the longitudinal phase space. As expected, the total longitudinal emittance can significantly exceed the emittance of the central part containing $\sim 80 - 85\%$ of the accelerated particles. For the parameters of the RFQ listed in Table I, the longitudinal emittance at the level of 99.9% is less than $2 \pi \cdot \text{keV/u} \cdot \text{nsec}$ for two-charge state uranium beam. This value was obtained from simulation of $5 \cdot 10^4$ particles with initial transverse normalized emittance $0.5 \pi \text{ mm} \cdot \text{mrad}$.

IV. ELECTROMAGNETIC FIELD OF THE LOW- β SC RESONATOR

The simulation of beam dynamics in the presence of all components of both electric and magnetic field is essential in superconducting quarter-wave resonators (SC QWR). The driver linac will use ~ 80 QWRs operating at 57.5 MHz and 115 MHz. Electrodynamics studies of the field distributions in the beam-cavity interaction area indicate appreciable dipole components of both electric and magnetic fields, especially for higher-frequency cavities [20]. The dipole fields induce beam steering, which is a strong function of rf phase and which couples the longitudinal and transverse motion resulting in transverse emittance growth. Such emittance growth cannot be compensated by static fields and can be a particularly serious problem in applications for beams with high charge-to-mass ratio. For example, the low-beta section of the driver linac can be retuned to provide a maximum energy gain of 46 MeV for protons. This regime is most sensitive to beam steering by the dipole components of electromagnetic field. We have analyzed and proposed two possible methods for the correction of such dynamic beam-steering effects in quarter-wave resonators (QWR) [15]. Simply offsetting the cavity beam-axis by 1-2 mm can often provide adequate compensation. In this method, the available range of steering is limited by the reduction of useful aperture. Offsetting can be effectively applied for low-intensity heavy-ion accelerators dealing with $q/A < 1/3$ in velocity range $\sim 0.01c - 0.15c$. This method will be used, for example, in the ISAC-II project [21]. More generally, steering can be largely eliminated over the entire useful velocity range by shaping the drift-tube and cavity wall faces adjacent to the beam axis to provide appropriate corrective vertical electric field components. This method is being applied in a 115 MHz QWR resonator being developed for the RIA driver linac [4]. In some cases steering is sufficiently small that the QWR can be used without any correction. For example, a plan for the pre-stripper section of the RIA driver linac calls for ~ 37 uncorrected 57.5 MHz QWR cavities [15]. Due to the low frequency, the steering component of the magnetic field is strongly suppressed. Even for a beam of protons there is no appreciable emittance growth because the longitudinal emittance of the beams in the RIA linac is small [5] and the beam center displacement remains less than 2 mm along this section of the linac. Beam center displacement for heavier ions is much less than for protons. Figure 3 shows the 115 MHz QWR and 172.5 MHz $\beta_G = 0.252$ half-wave resonator (HWR) being developed for the RIA driver linac. Beam

steering effects vanish in half-wave resonant cavities, since there are no dipole fields on the beam axis.

There is, however, another problem in QWR drift-tube design caused by quadrupole terms in the transverse Lorentz force which can cause appreciable emittance growth when the linac lattice includes transverse focusing by SC solenoids [22]. Solenoidal focussing provides a compact lattice and maximizes transverse acceptance while maintaining low longitudinal emittance. Early SC resonator designs for accelerating heavy-ions included large diameter drift tubes to provide axial symmetry of the electric field in the beam aperture. Some recent QWR designs have eliminated the drift tube, perforating the cylindrical central stems. The reduced cylindrical symmetry around the beam axis introduces an appreciable quadrupole component of transverse rf field. Detailed analysis shows that the transverse effect of electric field in the accelerating gap can be represented as a sum of axially symmetric and quadrupole lenses. Rf field properties of several geometries of QWR and HWR SC cavities and the impact of field asymmetries on beam quality have been studied by computer simulations of beam dynamics in realistic three-dimensional electromagnetic fields. Beam parameters have been analyzed for several typical examples of accelerating-focusing lattice. We find that beam steering due to the dipole component of the rf field and emittance growth due to the quadrupole field component in the aperture can be largely avoided by the appropriate design of the SC resonators [15].

V. FOCUSING LATTICE DESIGN IN SC LINACS

In SC linacs focusing elements alternate with accelerating cavities. In the design of the periodic focusing lattice of the SC linac several important issues should be taken into account. Standard criteria such as stability of the transverse motion and maximum possible acceptance certainly should be applied. In SC linacs, due to the high accelerating gradients available from SC cavities and the relatively long focusing periods, strong interactions between transverse and longitudinal motion may occur. Long focusing periods containing several cavities per period decrease the cost of the accelerator. However, in some lattice designs, the transverse-longitudinal coupling can excite a parametric resonance of transverse oscillations [23]. The condition for an n -th order parametric resonances of transverse motion is $\mu_t = \frac{n}{2}\mu_l$, where μ_t and μ_l are the phase advances of the transverse and longitudinal oscillations per focusing period. The analysis of parametric resonances is usually done in a smooth approximation of the equation of motions [19] written in the unitless variable $d\tau = \frac{\beta c}{S_f} dt$, where S_f is the length of the focusing period. What follows is based on this theory. The accelerating field is represented as an equivalent traveling wave with a positive stable equilibrium phase. For a given n , the resonance width is determined by

$$a_n \Delta_s < \mu_t^2 < b_n \Delta_s, \quad (2)$$

where a_n and b_n are the boundaries of the stability region in the solution of Mathieu's equation. The defocusing factor Δ_s is given by the expression:

$$\Delta_s = \frac{\pi q}{2 A} \frac{1}{(\beta_s \gamma_s)^3} \frac{S_f^2}{\lambda} \frac{e E_m \sin \varphi_s}{m_u c^2}, \quad (3)$$

where γ is the relativistic factor, λ is the wavelength of rf field and E_m is the amplitude of the equivalent traveling wave of the accelerating field. If we assume that the amplitude of the longitudinal phase oscillations Φ to be equal to the equilibrium phase angle $\Phi = \varphi_s$, then for $n=1$

and $\varphi_s=30^\circ$ one can obtain $a_1 \approx 0$, $b_1 \approx 1.79$ [24]. For $n=2$ these values are $a_2 \approx 3.93$, $b_2 \approx 4.31$. The subscript s denotes the equilibrium particle. The longitudinal phase advance per focusing period is approximated by $\mu_l = 2\sqrt{\Delta_s}$.

The focusing structure of the linac can be considered as a periodic structure of the linac containing a given type of SC resonator. Irregularities in the periodic structure due to the inter-cryostat drift spaces can be compensated by the absence of the first SRF cavity in the very first focusing period of the cryostats [5]. Table II shows the accelerating-focusing structure of the baseline design of the driver linac. In the table, N_R is the number of SC resonators per focusing period and β_G is the geometrical beta of the cavity. The low- and medium- β of the linac contain drift tube SC cavities (DTL) and the 805 MHz section comprises elliptical cavities (ECL). The amplitude of the equivalent traveling wave of the accelerating field E_m varies significantly along the linac due to the many different types of SC resonators. The typical range of the average field E_m in the RIA driver linac is 1.5-5.0 MV/m. The parameters E_m , S_f , q/A in (2) and (3) are strong functions of the beam energy. Figure 4 shows the boundary values $\sqrt{a_n \Delta_s}$ and $\sqrt{b_n \Delta_s}$ ($n=1,2$) of the transverse phase advance, μ_t , along the linac calculated according the expression (2). If μ_t lies between these boundary values a parametric resonance can be excited.

In general, the phase advance per focusing period of transverse oscillations is optimized to provide the highest acceptance. For many periodic structures this condition occurs at $\mu_t \approx 65^\circ - 80^\circ$. The increase of μ_t above this value is inexpedient due to the growth of the beam envelope modulation factor which results in less transverse acceptance. In addition, the focusing structure becomes more sensitive to errors and misalignments for large values of μ_t . As can be seen in Fig. 4 the highest tolerable value of μ_t occurs in the first section of the ECL. In the baseline design of the RIA driver linac this section contains four 6-cell, $\beta_G=0.49$ cavities per focusing period. However, as already mentioned in ref. [5] a focusing period containing three 6-cell cavities is preferable. In this case, the boundary values of the transverse phase advance in Fig. 1 drop to values similar to those in the second section of the ECL.

The above-mentioned results were obtained from linear theory of particle motion. Extensive numerical simulations have been conducted in order to study the stability of transverse motion in the RIA driver linac for different focusing periods and transverse phase advances. For these simulations we use the code TRACK. The overall linac design is similar to the SC linac described in ref. [4]. As an example Fig. 5 shows the results of simulation in the medium- β section which starts with a 9.2 MeV/u uranium beam with the longitudinal emittance 30π keV/u-nsec taken intentionally to be 3 times larger than the expected emittance. Note that even this large emittance is well below the longitudinal acceptance of this linac section. The transverse phase advances and required focusing fields have been calculated both by applying first-order matrix formalism and with the code TRACE [25]. In TRACE the transverse phase advance was obtained without the beam rotations in the solenoids. In TRACK, however, the realistic fields of the solenoids were included. As expected from the diagram in Fig. 4 the transverse motion is unstable for $\mu_t=30^\circ$ in the beginning of 172.5 MHz section of the linac. In this case the resonance is strong and the energy of longitudinal oscillations transforms to transverse oscillations as is seen from the rms emittance behavior in Fig. 2. For stronger focusing, $\mu_t=40^\circ$ and 50° , the emittance growth is completely suppressed.

In the design of SC linacs parametric resonances in transverse motion must be identified and avoided. The transverse emittance growth of the beam is more pronounced for larger longitudinal emittances. The parametric resonance can result in the formation of beam halo in transverse

phase space if appropriate measures are not applied. In the RIA driver linac baseline design a transverse phase advance in the range 60° - 80° is recommended for the DTL. A phase advance μ_t close to 90° is preferable in the ECL. The results are valid for the selected lengths of the focusing periods of the RIA driver linac. Similar analysis techniques should be applied for different structures of the focusing period in SC linacs.

VI. DESIGN OF SC SECTIONS OF THE LINAC

VI.1. Accelerating-focusing lattice

The baseline design of the driver linac was described in ref. [5]. Below we present the latest modifications of the driver linac design which includes: 1) peak surface electric field in all drift-tube SC resonators assumed to be equal 20 MV/m except first seven 4-gap “ATLAS type” resonators; 2) the high- β section of the driver linac contains triple-spoke resonators (TSR) instead of elliptical resonators operating at the same value of peak electric field 28 MV/m [4].

Except the first cryostat which contains seven 4-gap resonators and one 2-gap resonator, the linac consists of 6 different types of cryostats filled by five different types of resonators as is seen from Fig. 6. Main parameters of the accelerating-focusing lattice and uranium beam energy along the linac are given in Table III. The linac consists of 352 SC cavities distributed in 68 cryostat modules. Table 3 does not show the parameters of the first cryostat. Transverse focussing is provided by SC solenoids contained in the same cryostat modules as the cavities. Such an array, with the cavities operated at a synchronous phase $\varphi_S = -30^\circ$ or -25° , provides strong focussing in both transverse and longitudinal phase space. Note, that the focusing lattice length is different for each of the four types of SRF cavities. Final adjustment of the longitudinal matching is done by choosing the appropriate value of synchronous phase.

The focusing period of the first three types of cryostats contains two or three cavities per period except for the first period which forms a focusing period with a “missing” cavity. The space of the missed cavity is replaced by the inter-cryostat drift. The flange-to-flange distance between the elements located in adjacent cryostats is set to be 50 cm. The focusing structure with the “missing” cavity is extremely helpful for tuning of beam motion in the transverse phase space. A little adjustment of the focusing fields in outermost solenoids is required in order to match beam. A similar focusing structure is designed for the cryostats containing 115 and 172.5 MHz SRF cavities.

VI.2. Stripper sections

The driver linac requires two charge-stripping sections. The passage of the high intensity heavy ion beam through the stripping film or foil results in several effects:

- At the exit of the stripping foil, the ion beam is a mixture of several charge states, with a Gaussian distributed intensity.
- The stripping foil experiences high thermal load, especially at the first stripper. A liquid lithium film for the first stripper is under development [26], both to accommodate the thermal load, and also to produce higher charge states.
- The average energy of the ion beam is slightly decreased due to ionization losses in the stripper.
- The transverse and longitudinal beam emittances are increased due to the energy straggling and scattering.

In order to avoid beam losses in the high-energy section of the Driver Linac the low-intensity unwanted charge states must be carefully separated and dumped. As long as the driver linac is designed for acceleration of multi-q beams, the beam transport system following the stripping foil must provide simultaneous matching of selected charge states to the six-dimensional acceptance of the following SRF linac [27]. This magnetic transport system (MTS) requires dipole magnets and a rebuncher in order to provide a proper transformation of the 6-dimensional beam emittance. The system must have a dispersive area, effectively operating as a spectrometer. In the region of maximum dispersion, the unwanted charge states are removed by horizontal beam collimation. We have designed such systems for both stripping areas. Several options for the MTS design can satisfy the above requirements. The options chosen here seem to best satisfy the overall architectural requirements of the linac. For example, after the first stripper, it is convenient to transversely shift the linac beam axis: the MTS incorporates two 90° bends to provide a 7.2m shift. After the second stripper it is economical to bend the beam through 180° , since such a bend greatly shortens the overall length of the linac tunnel (see fig. 1). The 180° bend shown in Fig. 7 provides for high-dispersion regions in the MTS which enable separation of low intensity charge states and cleaning or scraping of any beam halo. At the final stage of the MTS design, the higher order terms were included and corrected as necessary. Following the second stripper uranium charge states with $q = 88, 89, 90,$ and 91 will continue on through the system.

VI.3. Beam dynamics simulations

Beam dynamics in the SRF linac were numerically simulated using the TRACK code. The initial phase space distribution used for each charge state was taken to be the distribution at the exit of the RFQ as simulated by the DYNAMION code [18]. Figure 8 shows the longitudinal acceptance and two-charge state uranium phase space at the entrance of the SRF linac. Note, that the longitudinal effective emittance of 100% two charge-state uranium beam is $2.32 \pi \cdot \text{keV}/u \cdot \text{nsec}$. In longitudinal phase space, the emittance of the two charge-state beam is always larger than for a single charge-state beam. Growth in effective emittance occurs due to the oscillations caused by the slightly differing off-tune synchronous phases for the two charge states 28^+ and 29^+ . The effective emittance of a two charge-state beam oscillates along the low- β section of the linac as is seen from Fig. 9. A frequency jump by a factor of two at ~ 30 m does not introduce an additional emittance growth due to favourable beam parameters in this transition. Although the effective emittance value can be ~ 3.5 times larger than the input emittance, the total emittance of the two charge-state beam remains well inside the stable area in longitudinal phase space. The beam energy exiting low- β section should be selected in order to obtain the lowest effective emittance for the two charge-state beam. Similar reasons are applied for the selection of the uranium beam energy exiting medium- β section. Obviously this feature is very important to maintain low emittance along the whole driver linac.

Beam envelopes along the linac are shown in Fig. 10. The simulation was performed for two-charge state uranium in the low- β section, five charge states in the medium- β and three charge states in the high- β section. The multi-q MTSs were optimized up to third order.

VI.4. Effect of errors on beam parameters

All errors are randomly generated as a uniform distribution with the rms values δ_i listed in Table III. Accordingly the interval of the error distribution is $\pm \sqrt{3} \cdot \delta_i$. The sensitivity of multi-q beam parameters to various types of random errors and misalignments were studied by the ray-

tracing code TRACK. The most essential errors affecting transverse beam motion are the misalignments of transverse position of focusing elements. Due to the strong defocusing of low velocity particles by the SRF cavities the misalignments of the SRF cavities were taken into account too. Monte Carlo simulations of the dynamics of multi-q beams in the presence of alignment errors have been performed. We introduced alignment errors by displacing separately both ends of each solenoid and SRF cavity in both X and Y by an amount in accordance with the displacement values given Table III. Then we tracked the multi-q beam through this portion of the linac and noted the increase in transverse emittance resulting from the positioning errors. As was discussed in ref. [5,7] multi-q beam requires corrective steering in order to avoid appreciable emittance growth. Therefore our simulation was done in the presence of steering elements along the linac. This entire simulation was then repeated two hundred times, each time with a different, random set of alignment errors. These studies show that in the worse scenario the total emittance growth of multi-q beam is less than a factor of four in transverse phase space.

Phase and amplitude fluctuations in SRF cavity fields are simulated in order to find their effect on longitudinal effective emittance of the multi-q beam. The error values listed in Table III are based on the experience of the ATLAS accelerator which is a 50 MV superconducting heavy-ion linac being operated at Argonne National Laboratory. Phase and amplitude errors of the rf field are fast fluctuations and produce effective emittance growth of multi-q beam. Phase space plots obtained during 200 seeds are accumulated and shown in Fig. 11 at the entrance of medium- β section of the linac. The emittance of two charge-state beam remains much smaller than the acceptance of the following linac section.

The results of this simulation are summarized in Table VI and Fig. 12. The latter shows longitudinal phase space plots accumulated during 200 random seeds. As is seen the multi-q uranium beam can be accelerated up to 400 MeV/u with a $\pm 0.25\%$ energy spread and a ± 35 ps time width. A longitudinal emittance of $75.8 \pi \cdot \text{keV/u-nsec}$ contains all particles shown in Fig. 12. However, in these simulations we have not included possible emittance growth due to beam strippers.

VII. CONCLUSION

We have continued to develop and improve the baseline design for the medium-energy entirely SC heavy-ion linac. Several novel features have been implemented into the baseline design. Detailed beam dynamics simulation has been performed for multi-q uranium beam from the source to the linac exit. These simulations have been iterated repeatedly with the design of overall linac architecture. The simulations, which include misalignments of focusing and accelerating elements and random errors of the rf fields, show that beam emittances are well below the six-dimensional acceptance throughout of the whole SC linac.

VIII. REFERENCES

1. K. W. Shepard, J.R. Delayen, C.M. Lyneis, J.A. Nolen, P.N. Ostroumov, J.W. Staples, J. Brawley, C. Hovater, M. Kedzie, M.P. Kelly, J. Mammosser, C. Piller and M. Portillo, *in the Proceedings of the 9th International Workshop on RF Superconductivity, Santa Fe, New Mexico, 1999*, edited by B. Rusnak, p.345.
2. C.W. Leemann, in Proceedings of the 2000 Linac Conference, Monterey, California, August 21-25, 2000, SLAC –R-561, edited by A.W. Chao, p.331.

3. J.A. Nolen. Proceedings of the XXI International Linear Accelerator Conference, Gyeongju, Korea, August 19-23, 2002, http://linac2002.postech.ac.kr/db/abstract/show_abs_sessid.php?auth_sessid=MO302.
4. K. W. Shepard. Proceedings of the XXI International Linear Accelerator Conference, Gyeongju, Korea, August 19-23, 2002, http://linac2002.postech.ac.kr/db/abstract/show_abs_sessid.php?auth_sessid=TH301.
5. P. N. Ostroumov. Phys. Rev. ST. Accel. Beams **5**, 030101 (2002).
6. P.N. Ostroumov, J.A. Nolen and K. W. Shepard, in Proceedings of the 2000 Linac Conference, Monterey, California, August 21-25, 2000, SLAC –R-561, edited by A.W. Chao, p.1018.
7. P.N. Ostroumov and K. W. Shepard, Phys. Rev. ST Accel. Beams **3**, 030101 (2000).
8. P.N. Ostroumov, R.C. Pardo, G.P. Zinkann, K.W. Shepard and J.A. Nolen, Physical Review Letters, **86**, N 13, p. 2798-2801 (2001).
9. P.N. Ostroumov, K. W. Shepard, V.N. Aseev and A.A. Kolomiets, in Proceedings of the 2000 Linac Conference, Monterey, California, August 21-25, 2000, SLAC –R-561, edited by A.W. Chao, p. 202.
10. M.A. Leitner, D.C. Wutte and C.M. Lyneis, in *Proceedings of the 2001 Particle Accelerator Conference, June 18-22, Chicago, IL, 2001*, p.67.
11. H. Wollnik, J. Brezina and M. Berz, NIM, **A258**, (1987) 408.
12. M. Berz, COSY INFINITY, Version 8 User's Guide and Reference Manual, MSU, 1999.
13. K. L. Brown, The ion optical program TRANSPORT. Technical Report 91, SLAC, 1979.
14. A.A. Kolomiets, V. Pershin, I. Vorobyov, S. Yaramishev and Ju. Klabunde, in *Proc. of the Sixth European PAC, Stockholm, Sweden, June 22-26, 1998*, edited by S. Myers et al., p. 1201.
15. P. N. Ostroumov and K. W. Shepard, Phys. Rev. ST. Accel. Beams **11**, 030101 (2001).
16. CST Microwave Studio, User Manual Version 3.0, January 2001, CST GmbH, Darmstadt, Germany. <http://www.cst.de/>.
17. S. Kowalski and H.A. Enge. RAYTRACE. MIT Report, July 1, 1987.
18. P.N. Ostroumov, A.A. Kolomiets , D.A. Kashinsky, S.A. Minaev, V.I. Pershin, T.E. Tretyakova, S.G. Yaramishev. Phys. Rev. ST Accel. Beams **5**, 060101 (2002).
19. I.M. Kapchinskiy, *Theory of Linear Resonant Accelerators* (Energoizdat, Moscow, 1982). (In Russian).
20. Facco and V. Zviagintsev, in Proc. of the 2001 PAC, Chicago, IL, 2001, p. 1095.
21. M. Pasini, R.E. Laxdal and P.N. Ostroumov. Proc. of the EPAC2002, Paris, June 2002, p. 933.
22. P.N. Ostroumov and K.W. Shepard. Proceedings of the XXI International Linear Accelerator Conference, Gyeongju, Korea, August 19-23, 2002, http://linac2002.postech.ac.kr/db/abstract/show_abs_sessid.php?auth_sessid=TU468.
23. P. N. Ostroumov. Proceedings of the XXI International Linear Accelerator Conference, Gyeongju, Korea, August 19-23, 2002, http://linac2002.postech.ac.kr/db/abstract/show_abs_sessid.php?auth_sessid=MO412.
24. I.M. Kapchinsky. Selected Topics in Ion Linac Theory. Lectures given at the University of Maryland at College Park. February-April 1993.
25. K.R. Crandall. Report LA-11054-MS. Los Alamos, 1987.
26. J. Nolen, C.B. Reed, A. Hassanein, M. Portillo and J.H. Norem, in Physics Division Annual Report 2000, ANL-01/19, ANL, Argonne, IL, 2001, p. 152.

27. M. Portillo, V.N. Aseev, J.A. Nolen and P.N. Ostroumov, in *Proceedings of the 2001 Particle Accelerator Conference, June 18-22, Chicago, IL, 2001*, p. 3012.

Figure 1. Elements of the proposed linac.

Figure 2. Initial particle distribution and separatrices of the longitudinal motion calculated for different amplitudes of transverse oscillations at the injection velocity $\beta = 0.00507c$.

Figure 3. 115 MHz QWR (the left picture) and 172.5 MHz HWR (the right picture) of the RIA driver linac.

Figure 4. Unstable regions (shaded areas) of the transverse phase advance due to first and second order parametric resonances as a function of uranium beam energy.

Figure 5. Rms emittance evolution along the 172.5 MHz section of the linac, $\mu_t=30^\circ$.

Figure 6. Layout of six different types of cryostats along the driver linac (not in scale).

Figure 7. System for selecting multiple q state beams through a 180° bend at 81 MeV/u.

Figure 8. Longitudinal acceptance of the low- β SRF linac. The blue and magenta dots show the longitudinal phase space plots of uranium beam with charge $q=28+$ and $q=29+$ obtained at the RFQ exit.

Figure 9. Rms longitudinal emittance variation of single- (red curve) and two-charge-state (blue curve) beams along the low- β linac.

Figure 10. Beam rms and total envelopes along the driver linac.

Figure 11. Longitudinal acceptance of the medium- β SRF linac. The blue dots show the longitudinal phase space plots of uranium beam with charge $q=28+$ and $q=29+$ accumulated during 200 seeds of the linac with random fluctuations of phases and amplitudes.

Figure 12. Phase space plots of four-charge-state uranium beam at the exit of the driver linac.

Table I. Main parameters of the RFQ.

Operating frequency	57.5 MHz
Average radius R_0	0.6 cm
Vane tip radius R_e	0.45 cm
Vane-to-vane voltage U_0	68.5 kV
Maximum field on the vane surface E_{\max}	140 kV/cm
Input beam energy	11.975 keV/u
Output beam energy	199 keV/u
Synchronous phase φ_s	-25°
Modulation factor	1.09 - 1.765
Aperture radius	0.43 cm
Phase advance of transverse oscillations σ_0	$44^\circ - 41^\circ$
Normalized transverse frequency Ω_r/ω , $\omega=2\pi c/\lambda$	0.123
Normalized longitudinal frequency Ω_l/ω	0.04
Normalized transverse acceptance	1.8π mm mrad
Ω_l/Ω_r	0.326
Vane length	392 cm
Longitudinal emittance at the exit of RFQ for 99.9% of particles	$2 \pi \cdot \text{keV/u} \cdot \text{nsec}$

Table II: Linac Structure

	f (MHz)	N_R	β_G	S_f (m)	Type of focusing
1	57.5	2	0.061	1.13	Solenoid
2	115	3	0.15	1.77	Solenoid
3	172.5	3	0.25	1.73	Solenoid
4	345	4	0.39	2.60	Solenoid
5	805	4	0.49	5.34	Doublet
6	805	4	0.61	5.84	Doublet
7	805	4	0.81	7.89	Doublet

Table III. Basic parameters of the lattice.

Cryostat type as is shown in Fig. 6	I	II	III	IV	V	VI
Frequency (MHz)	57.5	115	172.5	345	345	345
Cavity beta	0.061	0.15	0.252	0.50	0.50	0.62
Number of cryostats	4	5	12	8	12	26
Number of cavities	37 [*]	41 [†]	96	33 [†]	36	104
Length of focusing period (m)	1.13	1.77	1.73	2.38	3.98	5.80
Number of cavities per focusing period	2	3	3	2	3	4
Beam energy (MeV/u)	4.78	10.15	55.33	86.26	148.3	402.15
Aperture diameter (mm)	30	30	30	40	40	40
Synchronous phase (deg)	-30	-25	-30	-30	-30	-25
Type of cavity	QWR	QWR	HWR	TSR	TSR	TSR
Peak surface field (MV/m)	20	20	20	28	28	28
Accelerating field (MV/m)	5.71	5.41	6.45	8.45	8.45	8.45
Effective length of the SC solenoids (cm)	18	30	30	30	40	50
Focusing field of the SC solenoids (T)	6.6-9.2	8.3-11.0	5.8-8.6	8.6-9.5	6.8-10.0	8.7
RMS misalignments of the ends of the solenoid (mm)	0.17	0.17	0.17	0.17	0.17	0.17
Random RMS fluctuation of RF field phase (deg)	0.3	0.3	0.3	0.3	0.3	0.3
Random RMS fluctuation of the field amplitude (%)	0.3	0.3	0.3	0.3	0.3	0.3

^{*}Including one cavity located in the first cryostat.

[†]Including a cavity-rebuncher.

Table IV. Summary of longitudinal beam emittance at the exit of the driver linac.

	Emittance $\pi \cdot \text{keV}/\text{u} \cdot \text{nsec}$
4-RMS emittance	13.6
4-RMS emittance with errors	18.2
98% emittance with errors	33.5
100% emittance with errors	75.8

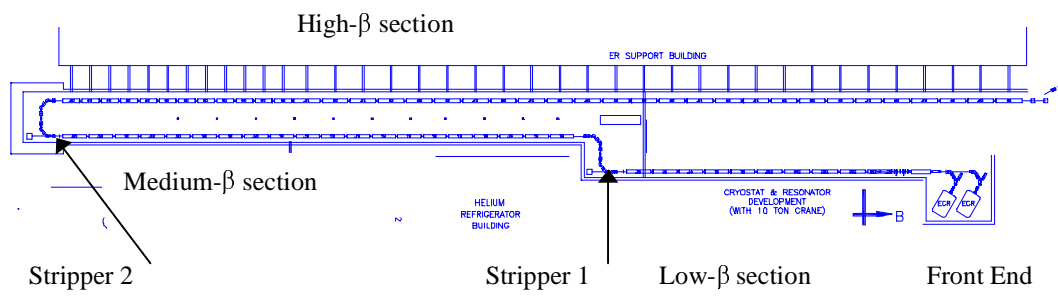


Figure 1.

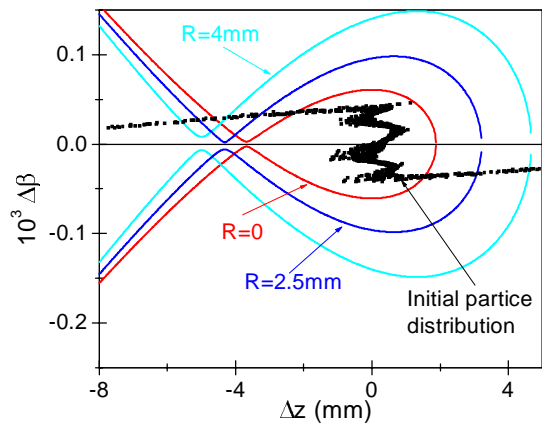


Figure 2.

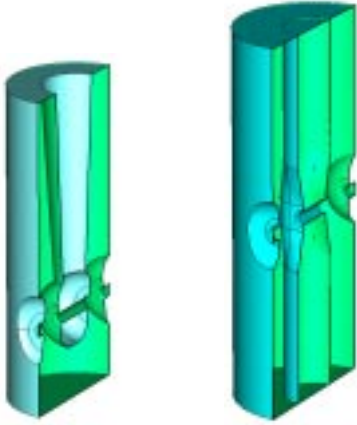


Figure 3.

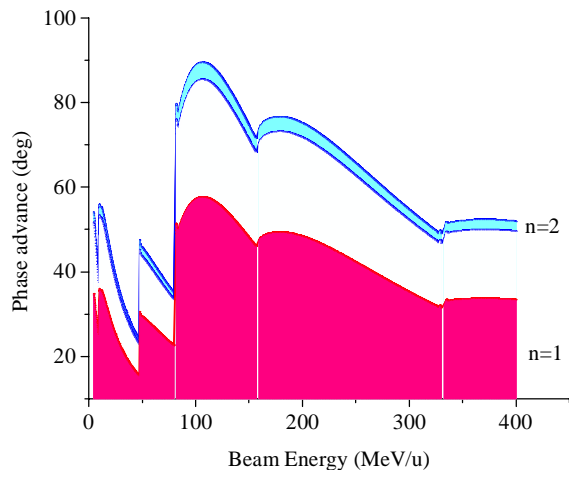


Figure 4.

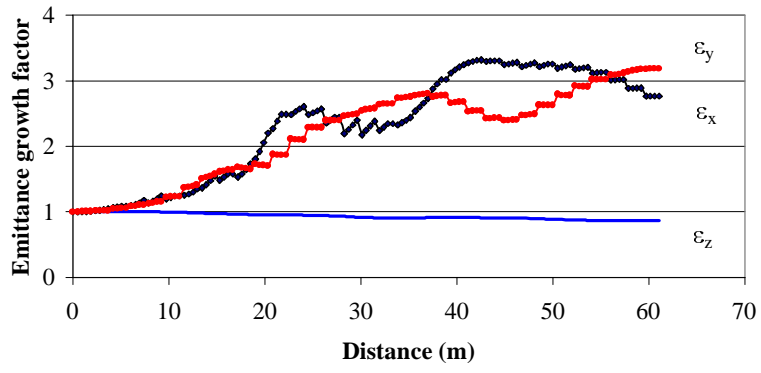


Figure 5.

Cryostat type

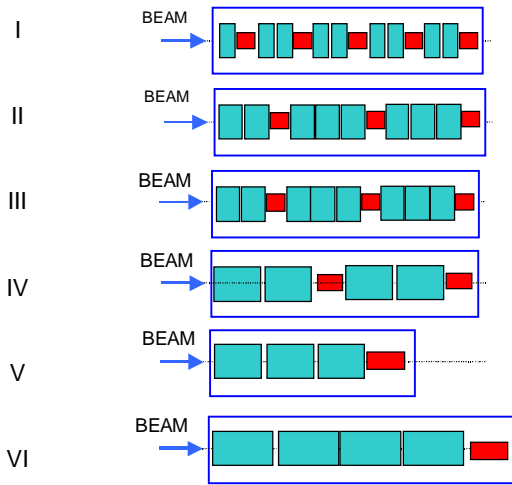


Figure 6.

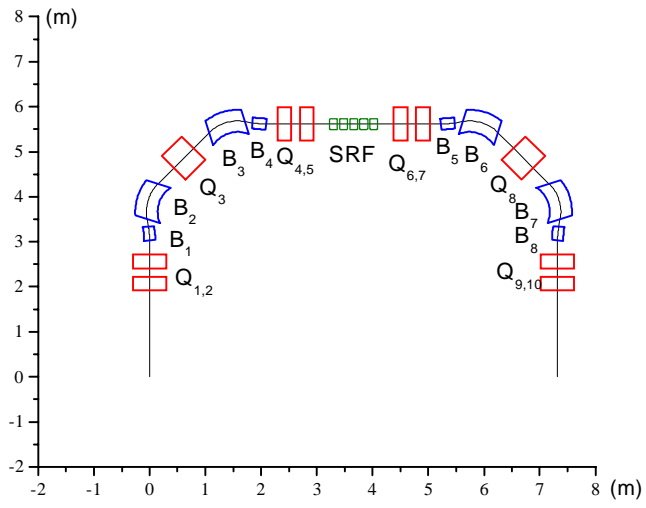


Figure 7.

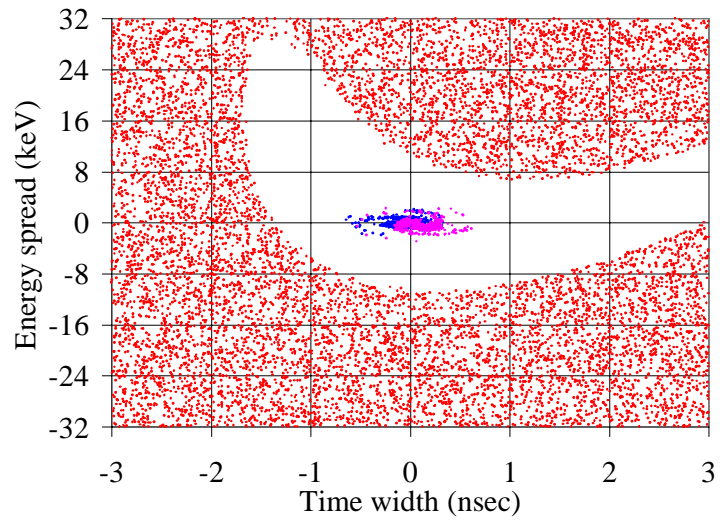


Figure 8.

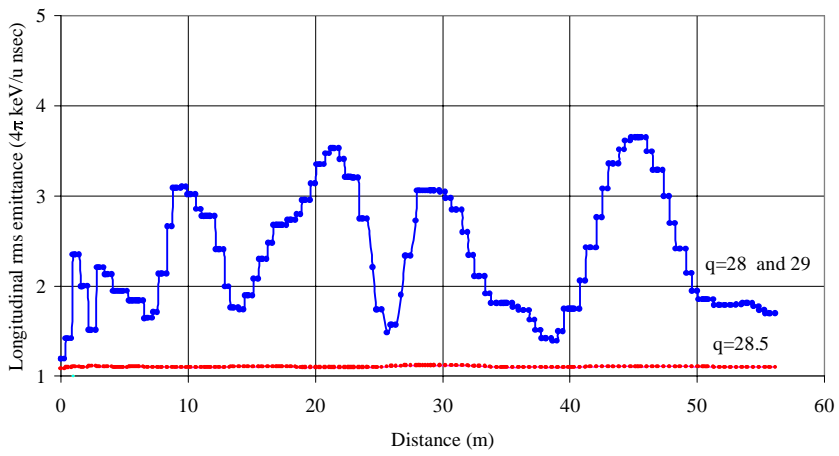


Figure 9.

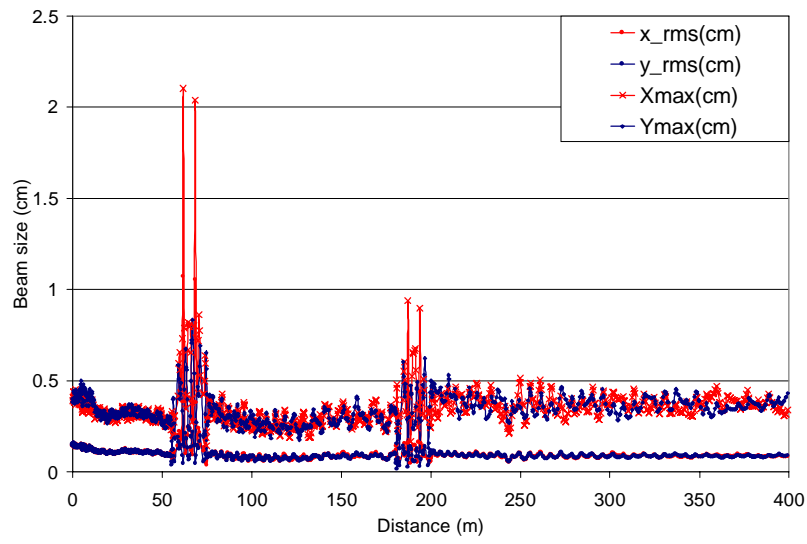


Figure 10.

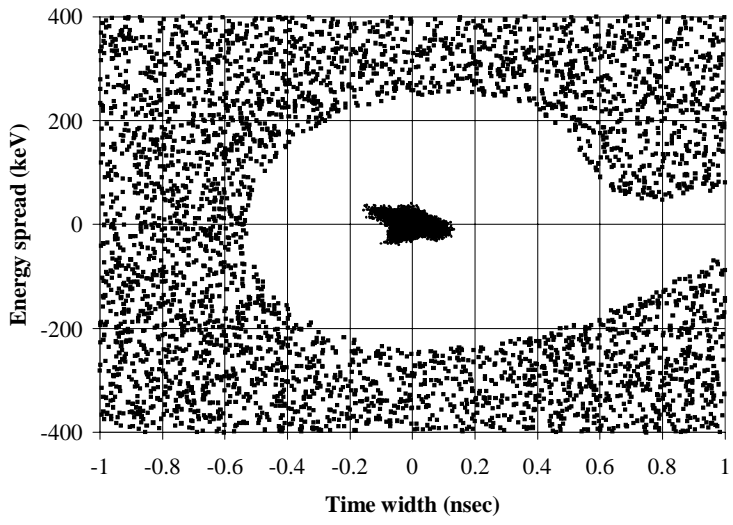


Figure 11.

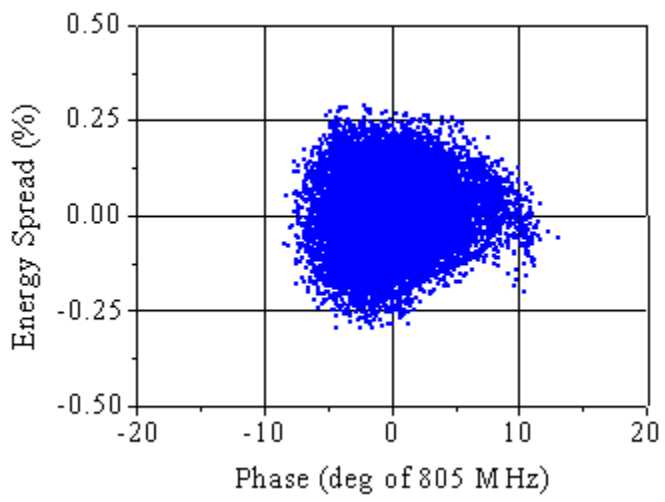


Figure 12.